

FRACTURE MECHANISMS OF EUTECTIC CRYSTALS PROCESSED BY DIRECTIONAL SOLIDIFICATION

J. Y. Pastor, P. Poza, and J. LLorca

Department of Materials Science, Polytechnic University of Madrid
E. T. S. de Ingenieros de Caminos, 28040 – Madrid, Spain

ABSTRACT

The fracture micromechanisms were studied in two eutectics crystals, $\text{Al}_2\text{O}_3\text{-ZrO}_2(\text{Y}_2\text{O}_3)$ and $\text{CaF}_2\text{-MgO}$, grown by directional solidification. Three-point bend and fracture tests were carried out in the first material, which exhibited a flexure strength at ambient temperature of over 1GPa. This was due to the fine eutectic microstructure, which reduced the size of the critical defects at the specimen surface, and to the elevated toughness of the eutectic composite. The investigation in the second material was focussed on the interaction of the matrix cracks with MgO fibres. The matrix cracks did not penetrate the fibres but deflected along the interface, a behaviour which offers a potential to improve the toughness and the thermal shock resistance.

INTRODUCTION

It is well established that phase distribution, size, and shape as well as interface characteristics play a crucial role in determining the behaviour of multiphase materials, and significant improvements in the properties are often associated with the development of novel microstructures. In this respect, eutectic crystals grown from the melt constitute a family of *in situ* composites with a very fine microstructure, an excellent bonding between the phases and microstructural stability up to temperatures approaching the eutectic temperature. In addition, directional solidification leads to crystals with an ordered microstructure where the phase size can be limited to a few microns in large zones. The small phase size together with the absence of grain boundaries in the transverse direction hinder the presence of defects, and increase significantly the mechanical properties of brittle ceramic eutectics, whose strength is controlled by the size of the largest flaw [1-2].

Further improvements in the mechanical performance of these materials require a detailed study of fracture micromechanisms, and this work was carried out in two eutectics crystals, $\text{Al}_2\text{O}_3\text{-ZrO}_2(\text{Y}_2\text{O}_3)$ and $\text{CaF}_2\text{-MgO}$, grown by directional solidification. The former material has been considered [3] for a new generation of reinforcing fibres which can retain their strength up to very high temperature (1400°C), and the investigation was aimed at identifying the microstructural features with limit the ambient temperature strength (> 1 GPa) of these oxide eutectic crystals. The $\text{CaF}_2\text{-MgO}$ system is primarily intended for optical applications, and the research was centred in the analysis of crack deflection at the CaF_2/MgO interface, which may be used to improve significantly the fracture toughness and the thermal shock resistance.

MATERIALS AND EXPERIMENTAL TECHNIQUES

The $\text{Al}_2\text{O}_3\text{-ZrO}_2(\text{Y}_2\text{O}_3)$ and the CaF_2/MgO eutectics were grown at the Instituto de Ciencia de Materiales de Aragón. The former was prepared from a powder mixture of 34.5 mol % of ZrO_2 , 3.5 mol % of Y_2O_3 and 62 mol % of Al_2O_3 , which was pressureless sintered at 1500 °C to obtain precursor rods. Traces of Cr^{+3} are usually present in commercial Al_2O_3 powders. Directionally solidified eutectic rods of 50-100 mm in length were grown

at 30 mm/hour from the precursor rods by the laser floating zone-method, as described elsewhere [4]. Two different microstructures were found along the rods. The first was formed of colonies of approximately 30 μm in diameter formed by a fine interpenetrating network of two phases, which were identified as tetragonal ZrO_2 and $\alpha\text{-Al}_2\text{O}_3$ using Raman spectroscopy [5]. They were elongated in the growth direction in the rod centre and their aspect ratio was around 3-4 (Figure 1a). The colony aspect ratio and the inclination from the rod axis increased with the distance to the centre. The colonies were surrounded by a thick boundary region, which contained coarse ZrO_2 particles ($< 10 \mu\text{m}$). Pores and cracks were detected in this boundary region (Figure 1b). The colony arrangement was substituted in some regions along the rods by a second microstructure formed by a homogeneous interpenetrating network of both phases, which also contained small, equiaxed pores. (Figure 2). The volume fractions of Al_2O_3 and tetragonal ZrO_2 were, respectively, 70% and 30% in both types of microstructure.

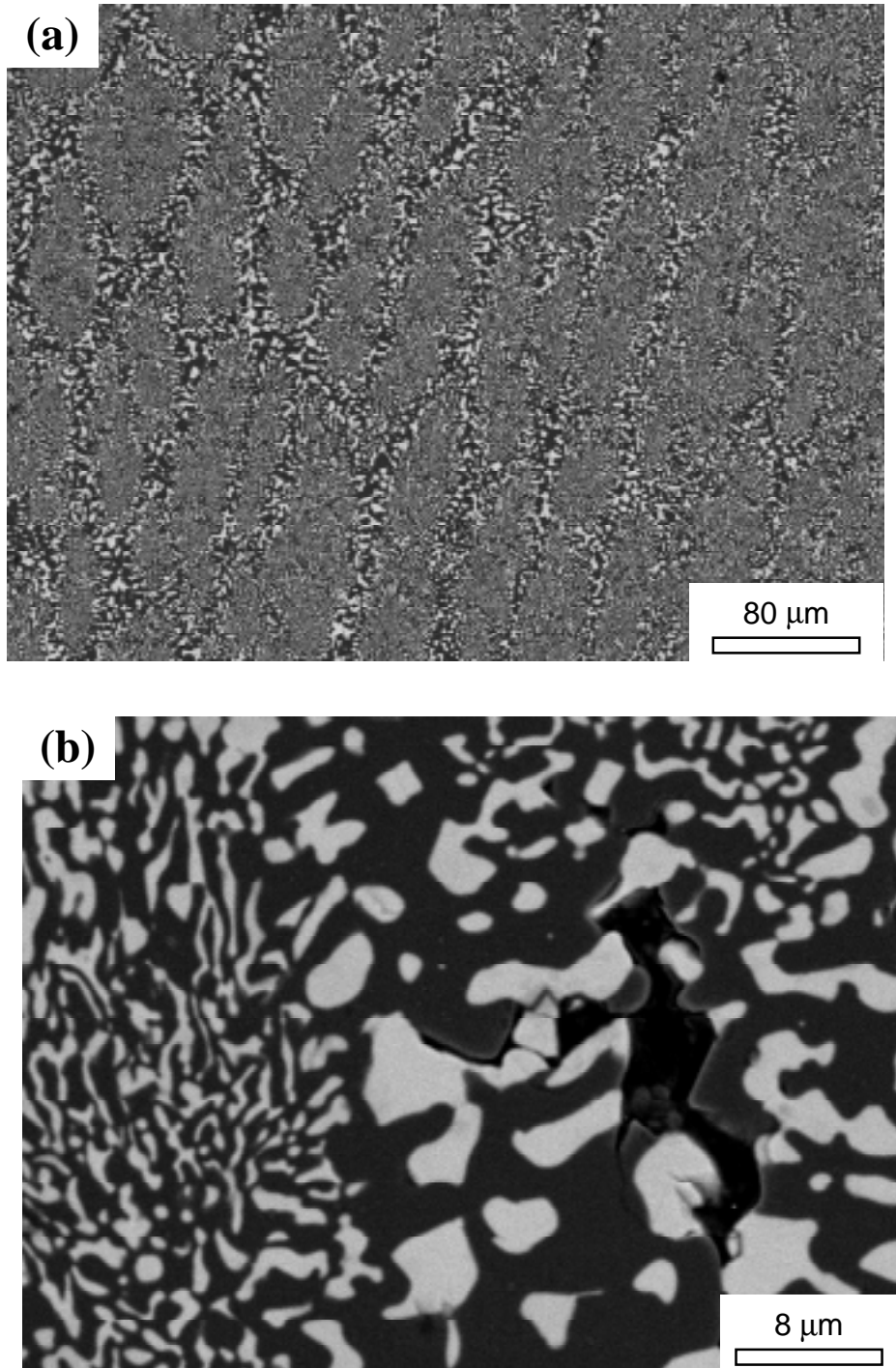


Figure 1: Colony structure in longitudinal sections of the $\text{Al}_2\text{O}_3\text{-ZrO}_2(\text{Y}_2\text{O}_3)$ rods. (a) General view near the

rod centre. (b) Detail of a crack at the colony boundary. Tetragonal ZrO₂ appears white and Al₂O₃ black. in the scanning electron micrographs.

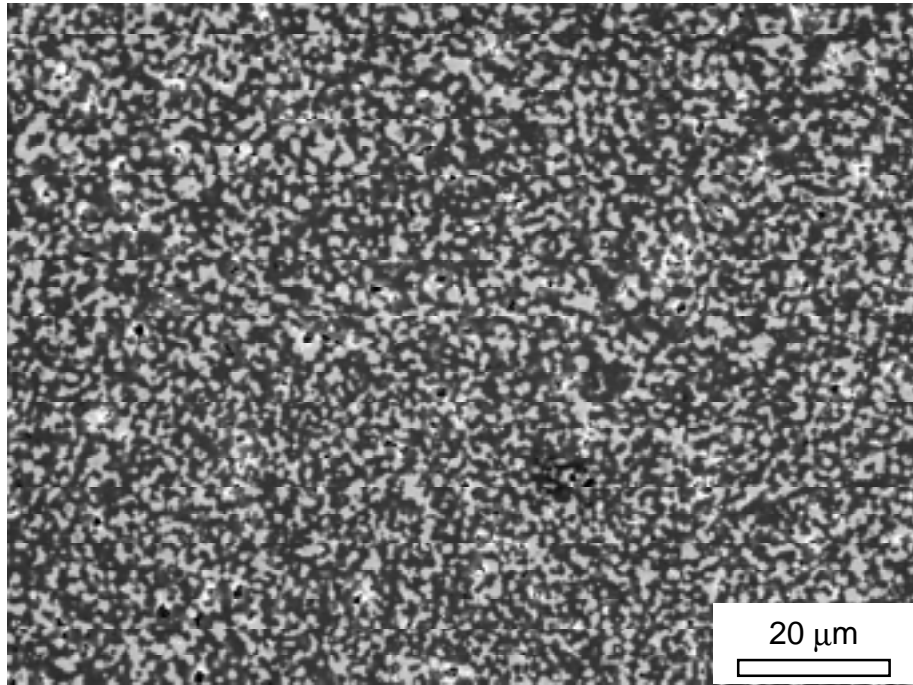


Figure 2: Interpenetrating network structure in longitudinal sections of the Al₂O₃-ZrO₂(Y₂O₃) rods. Tetragonal ZrO₂ appears white and Al₂O₃ black in the scanning electron micrographs.

The mechanical properties of the Al₂O₃-ZrO₂ eutectic were measured in rods of 1.3 mm in diameter. The dynamic elastic modulus in the longitudinal direction was determined by the flexural vibration resonance method on rods of 30 mm in length. The flexure strength was obtained through three-point bend tests performed under stroke control at a loading rate of 10 μm per minute. The span of the loading fixture was 5 mm. The flexure strength was computed from the maximum load in the test according to the Strength of Materials theory for an elastic beam of circular section. Finally, the fracture toughness was measured through tensile tests of notched rods. To this end, a straight notch with a root radius of around 180 μm was made in the rods with a diamond wire. The rod ends were introduced into cylindrical cavities machined in aluminium heads and glued to the aluminium. The heads were connected to the actuator and to the load cell of the testing machine using nylon cords, providing a very flexible loading system which ensured that the bending and torsional stresses on the rods were negligible. The notched rods were tested under stroke control at a cross-head speed of 2 mm per minute. The fracture toughness was computed from the maximum load in the test and from the notch length using the appropriate expression for the stress intensity factor [6].

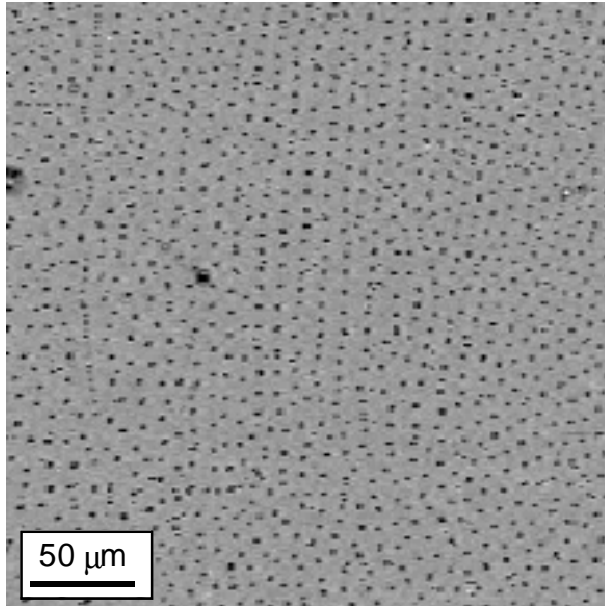


Figure 3: Transverse cross-section of the CaF_2/MgO eutectic. The MgO fibres were distributed in an imperfect hexagonal arrangement within the CaF_2 matrix.

Single crystals of CaF_2/MgO eutectic were grown by the Bridgman method in Ar atmosphere using a radio frequency furnace at 5 mm/hour, as described elsewhere [7]. The transverse cross-section of the directionally solidified eutectic is shown in Figure 3. It was formed by a homogeneous distribution of MgO fibres (0.5–0.8 μm in diameter) oriented parallel to the cubic axis of the CaF_2 matrix. Crack propagation was studied on polished transverse and longitudinal cross sections, where cracks were nucleated and propagated from microindentations performed at a load of 500 g.

STRENGTH AND TOUGHNESS OF $\text{Al}_2\text{O}_3\text{-ZrO}_2(\text{Y}_2\text{O}_3)$

The average values of the longitudinal elastic modulus, E , the flexure strength, σ_f , and the fracture toughness, K_C , are shown in Table 1, together with the corresponding standard deviations. The first interesting result in this table is the high value of the longitudinal elastic modulus, which is very close to the upper limit of 385 GPa predicted by the rule of mixtures from the volume fraction of each phase and their respective elastic moduli: 456 GPa in the $<0001>$ direction for Al_2O_3 [8] and 220 GPa for tetragonal ZrO_2 [9].

In addition, the mechanical properties of the $\text{Al}_2\text{O}_3\text{-ZrO}_2(\text{Y}_2\text{O}_3)$ rods were excellent. The flexure strength was approximately 30–40% higher than that reported by Homeny and Nick [10] on eutectics of equivalent composition processed by hot pressing. More recently, Sayir *et al.* [3] measured flexure strengths of • 2 GPa in fibres of the same composition processed by the edge-defined film-fed method. The diameter of these fibres was around 100 μm , which may explain the higher strength of these fibres as compared with that of the rods of 1.3 mm in diameter used in this investigation. These authors also studied the high temperature flexure strength and creep resistance of $\text{Al}_2\text{O}_3\text{-ZrO}_2(\text{Y}_2\text{O}_3)$, and concluded that the combination of strength, toughness, and thermal expansion coefficient of these fibres was very promising for use as reinforcement in intermetallic- and metal-matrix composites [3].

TABLE 1
MECHANICAL PROPERTIES OF $\text{Al}_2\text{O}_3\text{-ZrO}_2(\text{Y}_2\text{O}_3)$ EUTECTIC OXIDE

| E (GPa) | σ_f (MPa) | K_C (MPa \cdot m) |
|-------------|------------------|------------------------|
| 343 ± 7 | 1130 ± 50 | 7.8 ± 0.3 |

The excellent strength of this eutectic composite is due to the combination of a fine microstructure and a high toughness. Assuming that the surface defects leading to fracture behave as semicircular cracks, their critical radius, a_c , can be computed as [11]:

$$a_c = \frac{1}{\pi} \left[\frac{K_c}{0.65 \sigma_f} \right]^2 = 36 \mu\text{m.} \quad (1)$$

This value is of the same order as the diameter of the colonies in Figure 1, whose size might be considered in a first approximation as the critical microstructural parameter controlling the flexure strength. Other authors, however, found no increase in strength by reducing the colony size [1, 3]. They argued that the width of the colony boundaries, as well as the porosity in these regions, increases as the colony diameter decreases. As a result, the width of the colony boundaries becomes the critical factor for small colony sizes, and no improvements in strength were observed when the average colony size was reduced [1, 3].

Our analyses of the fracture surfaces concluded that fracture started from defects associated with longitudinal cracks formed during solidification (Figure 4). These longitudinal cracks appeared at the colony boundaries, and seemed to be associated with decohesions at the $\text{ZrO}_2/\text{Al}_2\text{O}_3$ interfaces (Figure 1b). Although the bonding between both phases is excellent, interface decohesion may be induced by the high thermal residual stresses developed upon cooling from the processing temperature as a result of the mismatch in thermal expansion coefficients between the phases. The magnitude of the average residual stresses in the alumina was obtained from the shift in position of the R_1 (14402 cm^{-1}) and R_2 (14432 cm^{-1}) intensity peaks in the luminiscence spectra of Cr^{+3} in Al_2O_3 in the rods, as compared with that of unstressed ruby [5]. The shifts can be related to the average residual stresses in the longitudinal (growth direction, $\sigma_{//}$) and transverse (σ_{\perp}) directions using the piezospectroscopic tensors of the R-line emission determined by He and Clarke for ruby in compression [12]. They are shown in Table 2, together with the hydrostatic stress component, σ_h (the \pm errors in the Table are statistical errors from the band shape fit). Al_2O_3 was subjected to compressive stresses within the eutectic composite, while tetragonal ZrO_2 was in tension. The magnitude of these stresses in ZrO_2 can be easily estimated through the self-consistent method [5], and the corresponding values are also shown in Table 2. The large difference between the stresses in each phase has to be accommodated at the interface, and it is not surprising that cracks propagated from pores or small flaws upon cooling from the processing temperature. Of course, the longer cracks were likely to develop and grow in the colony boundaries, where the ZrO_2 grains were bigger.

TABLE 2
AVERAGE RESIDUAL STRESSES IN EACH PHASE OF THE EUTECTIC OXIDE

| | $\sigma_{//}$ (GPa) | σ_{\perp} (GPa) | σ_h (GPa) |
|-------------------------|---------------------|------------------------|------------------|
| Al_2O_3 | -0.25 ± 0.4 | -0.42 ± 0.2 | -0.36 |
| ZrO_2 | 0.84 | 0.95 | 0.91 |

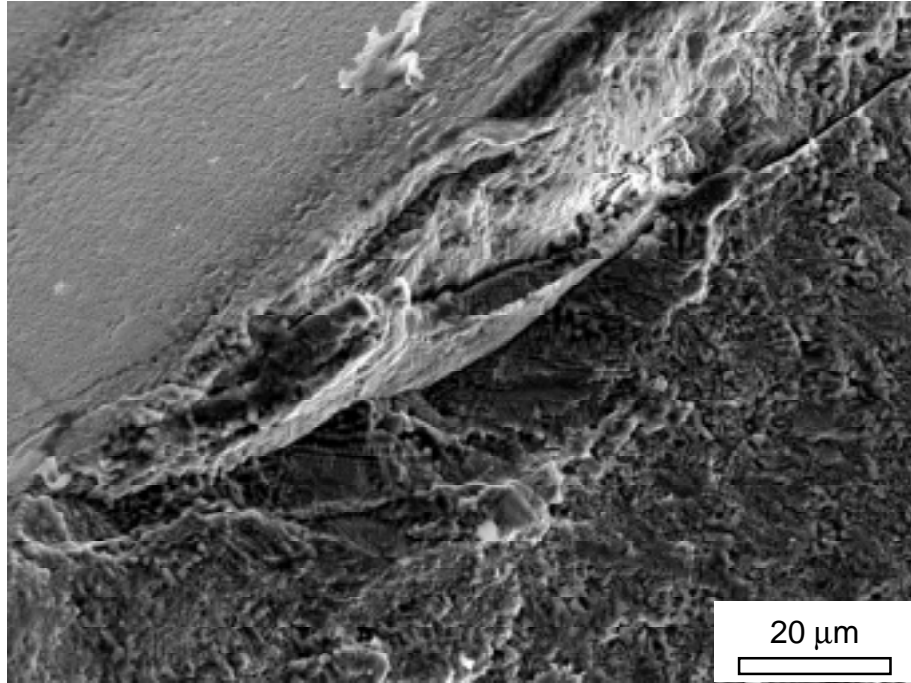


Figure 4: Fracture initiating flaw at the surface of an Al_2O_3 - $\text{ZrO}_2(\text{Y}_2\text{O}_3)$ rod tested in bending.

CRACK PROPAGATION IN CaF_2/MgO

The cracks nucleated from indentations propagated through the CaF_2 matrix. Their interaction with the MgO fibres is shown in Figures 5a and 5b, which correspond to transverse and longitudinal sections, respectively. These figures clearly show that the matrix cracks did not penetrate the MgO fibres but deflected along the fibre/matrix interface even in the worst scenario for crack deflection (as compared to crack penetration) which occurs when the crack propagates perpendicularly to the interface [13]. This behaviour ensures that the presence of the MgO fibres will improve the toughness and the thermal shock resistance of the CaF_2/MgO eutectic ceramic. If the matrix cracks penetrate the fibres, the overall behaviour of the composite is brittle as the matrix and fibres have very low fracture resistance. On the contrary, if the matrix cracks deflect along the fibre/matrix interface, they continue their propagation through the matrix without breaking the fibres. The non-broken fibres behind the crack front bridge the crack and slide with respect to the matrix. The elastic energy stored in the fibres, together with the energy spent pulling out the fibres which are eventually broken within the matrix, increase significantly the fracture energy of the composite, which may be over two orders of magnitude higher than that of the unreinforced ceramic matrix [14].

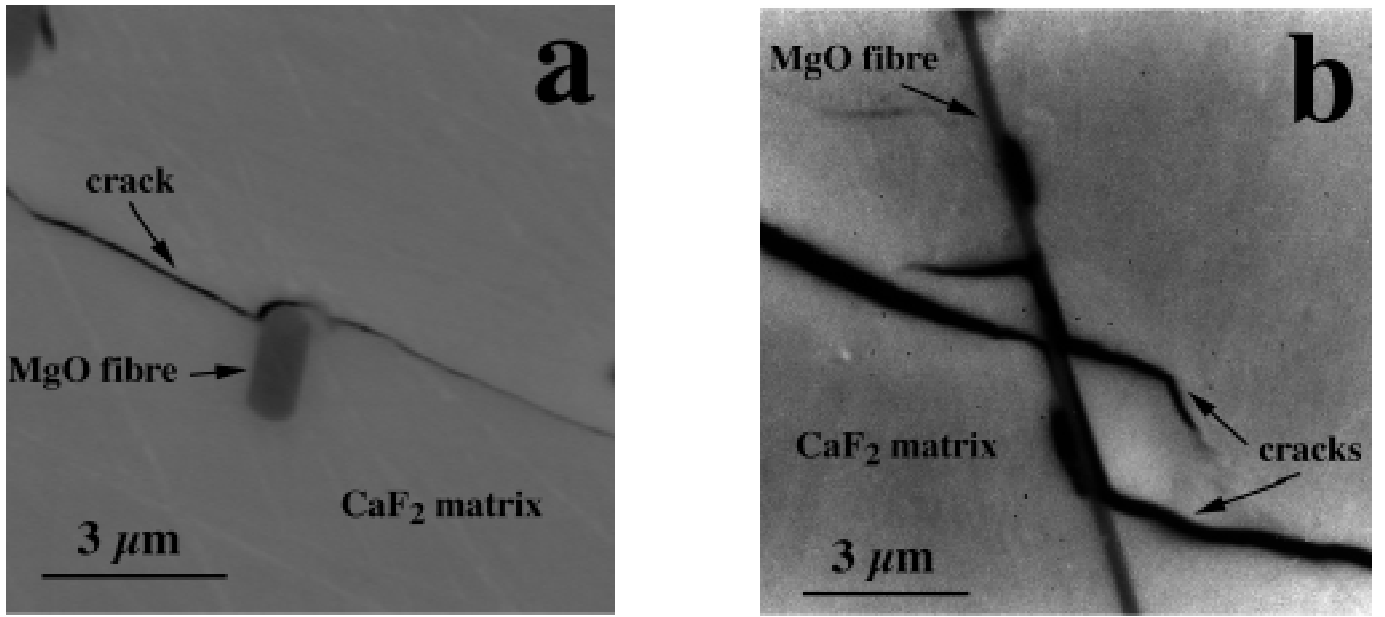


Figure 5: Back-scattered scanning electron micrographs showing crack deflection along the CaF_2/MgO interface. (a) Transverse section. (b) Longitudinal section.

The experimental results of crack deflection in Figure 5 can be rationalised by using the theoretical framework developed by He and Hutchinson [13]. The transition between crack deflection at the fibre/matrix interface and crack penetration into the fibre (assuming that both materials behave as isotropic elastic solids) is given by [13],

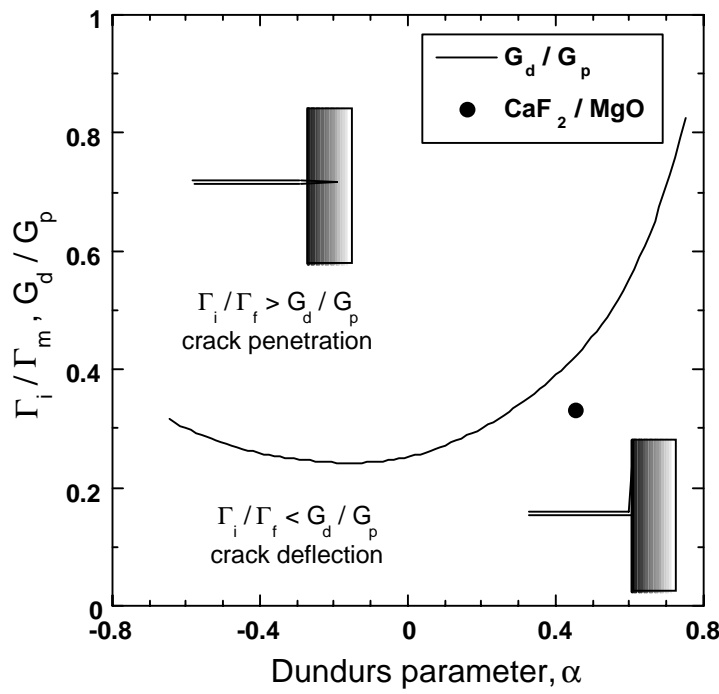
$$\frac{\Gamma_i}{\Gamma_f} = \frac{G_d}{G_p} \quad (2)$$

where Γ_i is the fracture energy of the interface and Γ_f stands for fracture energy of the fibre (Figure 6). G_d and G_p are the energies available to propagate the crack either along the interface (crack deflection) or through the fibre (crack penetration). The solution of equation (2) for a crack perpendicular to the interface is plotted in Figure 6 as a function of the Dundurs parameter α , which is given by

$$\alpha = \frac{E_f^* - E_m^*}{E_f^* + E_m^*} \quad (3)$$

where E_m^* and E_f^* are the matrix and fiber generalized elastic moduli, which are equivalent to the corresponding elastic moduli E in plane stress and to $E^* = E/(1-v^2)$ under plane strain conditions, v being the Poisson's ratio. The values of E and v for isotropic polycrystalline CaF_2 and MgO can be found in the literature [8] and are shown in Table 3. It should be noticed that equation (2) was obtained for isotropic elastic materials but it may be extrapolated to cubic crystals, whose degree of anisotropy is limited. For instance, the elastic moduli of the MgO fibres in the [110] and [211] direction are, respectively, 321 GPa and 286 GPa, very close to the average value for polycrystals.

Figure 6: Regions of crack deflection and crack penetration for a crack perpendicular to the interface. The



solid symbol corresponds to the CaF_2/MgO ceramic eutectic.

TABLE 3
ELASTIC CONSTANTS AND FRACTURE ENERGIES

| | E (GPa) | ν | $\Gamma (\text{J/m}^2)$ |
|----------------|---------|-------|-------------------------|
| CaF_2 | 110 | 0.30 | 0.5 |
| MgO | 310 | 0.18 | 1.5 |

The only experimental data for the fracture energy of CaF_2 and MgO single crystals were reported by Kingery *et al.* [15] and are also shown in Table 3. They correspond to cleavage fracture induced at 77 K. Results for the fracture energy of the CaF_2/MgO interface were not found, but the fracture energy of CaF_2 can be taken as an upper limit. According to these magnitudes for the elastic constants and fracture energies, the matrix cracks in the eutectic composite (represented by a solid symbol in Figure 6) should exhibit crack deflection at the fibre matrix interface, as was experimentally observed

CONCLUSIONS

The fracture micromechanisms were studied in two eutectics crystals, $\text{Al}_2\text{O}_3\text{-ZrO}_2(\text{Y}_2\text{O}_3)$ and $\text{CaF}_2\text{-MgO}$, grown by directional solidification. The former presented excellent flexure strength (1.1 GPa), which was attributed to the small size of the critical defects and to the elevated toughness ($7.8 \text{ MPa} \cdot \text{m}^{1.5}$) of the eutectic composite. Fractographic analysis showed that failure was nucleated in defects associated with longitudinal cracks formed during solidification in the colony boundaries. The micromechanisms of crack propagation were studied in single crystals of CaF_2/MgO eutectic. The matrix cracks did not penetrate the MgO fibres, but deflected along the fibre/matrix interface. This behaviour was rationalised by using the theoretical framework for crack deflection at an interface developed by He and Hutchinson [13], and it demonstrated the potential of MgO fibres to improve the toughness and the fracture resistance of CaF_2 single crystals.

Acknowledgements

The authors wish to express their gratitude to Prof. V. M. Orera, and Drs. R. I. Merino and J. I. Peña from the

Instituto de Ciencia de Materiales de Aragón, who prepared the eutectic crystals. Special mention should be made of Dr. A. Larrea, who carried out the indentation experiments in the CaF₂/MgO eutectics. The financial support from CICYT through grant MAT97-672-C02-02 is also gratefully acknowledged.

REFERENCES

1. Stubican, V. S., and Bradt R. C. (1981) *Ann. Rev. Mater. Sci.* **11**, 267.
2. Ashbrook, R. L. (1976) *J. Am. Ceram. Soc.* **60**, 428.
3. Farmer, S. C., Sayir, A., and Dickerson, P. O. (1993). In: *In situ Composites, Science and Technology*. pp. 167-182, TMS, Warrendale.
4. García, I, Peña, J. I., Merino, R. I., and Orera, V. M. (1998) *Bol. Soc. Esp. Cerám. Vidr.* **2-3**, 256.
5. Pardo, J. A., Merino, R. I., Orera, V. M., Peña, J. I., González C., Pastor, J. Y., and LLorca, J. (2000). *J. Am. Ceram. Soc.* **83**, in press.
6. Levan, A., and Royer, J. (1993) *Int. J. Fracture* **61**, 71.
7. Larrea, A., Contreras, L., Merino, R. I., LLorca, J., and Orera, V. M. (2000). *J. Mater. Res.* **15**, in press.
8. Tropf, W. J., Thomas, M. E., and Harris, T. J. (1995). In: *Handbook of Properties of Crystals and Glasses*, McGraw-Hill, New York.
9. Subbarao, E. C., (1981) In. *Science and Technology of Zirconia*, Vol. 3. pp. 1-24, (A. H. Heuer, and L. W. Hobbs, Ed.), The American Ceramic Society, Westerville.
10. Homeny, J., and Nick, J. J. (1990) *Mater. Sci. Engng.* **A127**, 123.
11. Newman J. C., and Raju, I. S. (1981) *Engng. Fract. Mech.* **15**, 185.
12. He, J., and Clarke, D. R. (1995) *J. Am. Ceram. Soc.* **78**, 1347.
13. He, M-Y., and Hutchinson, J. W. (1989) *Int. J. Solids Struct.* **25**, 1053.
14. LLorca, J., and Singh, R. N. (1991) *J. Am. Ceram. Soc.* **74**, 2882.
15. Kingery, W. D., Bowen, H. K., and Uhlmann, D. R. (1976) *Introduction to Ceramics*, John Wiley & Sons, New York.